Journal of Carcinogenesis
Covering Genesis to Therapeutics

Journal of Carcinogenesis, ISSN: 1477-3163
2025; Vol 24: Issue 4s, https://carcinogenesis.com/

Sonication-Assisted Synthesis, Characterization and Dual Functional Performance of Ag_2O And Pani–Ag_2O Nanocomposites

P. Jenifer [1], P. Rajesh Anantha Selvan [*2]

[1]Research Scholar (20121272032006), Department of Chemistry, St. John's College, Palayamkottai, Tirunelveli, Affiiated to Manonmaniam Sundaranar University, Tirunelveli, Tamil Nadu, India.

[*2]Associate Professor, Department of Chemistry, St. John's College, Palayamkottai, Tirunelveli, Affiliated to Manonmaniam Sundaranar University, Tirunelveli, Tamil Nadu, India.-627003

Email ID: sankardhanekula3@gmail.com

***Corresponding Author:**

Rajesh Anantha Selvan

Email ID: rajesh.chem@st.johnscollege.edu.in

ABSTRACT

PANI/Ag_2O nanocomposites with varying Ag_2O weight percentages were synthesized via *in-situ* chemical oxidative polymerization using ammonium persulfate (APS) in acidic medium at room temperature. Structural and optical characterizations were carried out using PXRD, UV–Vis, and FTIR. Photocatalytic studies revealed that PANI/Ag_2O achieved the highest degradation efficiency (~70%) for methylene blue and Congo red dyes under visible light irradiation. The improved performance is attributed to the synergistic effect between PANI and Ag_2O, enhancing visible light absorption and suppressing electron–hole recombination. Additionally, the nanocomposites exhibited significant antimicrobial activity against Gram-positive and Gram-negative bacteria as well as pathogenic fungi Streptococcus aureus, Klebsiella pneumoniae, Pseudomonas aeruginosa and Fungi Candida albicans, Aspergillus niger, Aspergillus Flavus.

Keywords: *PANI/ Ag_2O, Nanocomposites, Photo degradation, antimicrobial activity*

How to Cite: P. Jenifer, P. Rajesh Anantha Selvan, (2025) Sonication-Assisted Synthesis, Characterization and Dual Functional Performance of Ag_2O And Pani–Ag_2O Nanocomposites, *Journal of Carcinogenesis*, *Vol.24, No.4s*, 74-85

1. INTRODUCTION

The development of multifunctional nanomaterials has received significant attention due to their potential applications in environmental remediation and biomedical fields. Metal oxides such as silver oxide (Ag_2O) have been widely investigated owing to their strong redox properties, tunable band gap, excellent catalytic, antifungal and antimicrobial activities (Kumar et al., 2017; Porramezan and Eisazadeh, 2011; Thenmozhi et al., 2013) . However, pristine Ag_2O nanoparticles often suffer from photocorrosion, agglomeration, and limited reusability, which restrict their performance in practical applications.

To overcome these limitations, the incorporation of conducting polymers such as polyaniline (PANI) into Ag_2O frameworks has emerged as a promising strategy. PANI not only enhances the charge separation and electron transfer efficiency but also provides structural stability, surface functionality, and an extended π-conjugated system that can synergistically improve the photocatalytic and antimicrobial properties of the composite (Abirami and E, 2024; Kumar et al., 2020; Rather et al., 2022; Shivhare and Vyas, 2017).

Characterization of the synthesized nanomaterials plays a vital role in understanding their structure–property relationships. Techniques such as UV–Vis diffuse reflectance spectroscopy (UV–DRS), FTIR spectroscopy, X-ray diffraction (XRD), and scanning electron microscopy (SEM) provide insights into the band gap energy, functional group interactions, crystallinity, morphology, and particle size distribution. These features directly influence the optical and catalytic efficiency of nanomaterials. For instance, tailoring the band gap and Urbach energy helps improve visible-light-

driven photocatalysis, while controlled surface chemistry enhances antimicrobial interactions.

The photocatalytic performance of Ag_2O and PANI–Ag_2O nanocomposites was evaluated against hazardous dyes such as methylene blue and congo red, which are widely used in textile and industrial processes and pose serious risks to aquatic ecosystems due to their non-biodegradable nature. Photocatalytic degradation using nanocomposites under visible light provides an eco-friendly approach for wastewater treatment, enabling effective mineralization of organic pollutants into less harmful byproducts (Li et al., 2014).

In addition to environmental applications, the antimicrobial potential of these nanomaterials was assessed against pathogenic bacterial (*Staphylococcus aureus, Klebsiella pneumoniae, Pseudomonas aeruginosa*) and fungal (*Candida albicans, Aspergillus niger, Aspergillus flavus*) strains. The synergistic mechanism of silver ion release, ROS generation, and PANI-assisted electrostatic interactions contributes to broad-spectrum antimicrobial efficacy, providing an added advantage for biomedical applications.

Thus, this chapter presents a comprehensive evaluation of the synthesized Ag_2O and PANI–Ag_2O nanocomposites, focusing on structural characterization, optical properties, photocatalytic dye degradation efficiency, and antimicrobial activity, thereby demonstrating their potential as multifunctional nanomaterials for environmental and biomedical applications.

2. MATERIALS AND METHODS

2.1 Synthesis of Polyaniline

Polyaniline (PANI) was synthesized using the sonication method. Initially, 9 mL of aniline (1 M) was mixed with 3 mL of hydrochloric acid (1 M) and stirred for 20 minutes to form aniline hydrochloride. Subsequently, 0.1 M ammonium persulfate (APS), was added dropwise to the solution under continuous stirring at 50 °C. The polymerization process was maintained for 4 hours to ensure complete conversion. The resulting precipitate was filtered, thoroughly washed with deionized water and acetone, and then dried in an oven at a constant temperature for 24 hours to yield a homogeneous polyaniline composite.

2.2 Synthesis of PANI- Ag_2O Nanocomposites

The PANI–Ag_2O binary nanocomposite was synthesized using the chemical oxidative polymerization method, in which aniline monomer was polymerized in the presence of Ag_2O, hydrochloric acid (HCl), and ammonium persulfate (APS) used as the oxidizing agent. The -to-aniline molar ratios were varied at 5%, 10%, 15%, and 20%. Initially, 20 mL of 0.2 M APS solution was added dropwise to a 0.1 M aniline hydrochloride solution containing Ag_2O nanoparticles, while maintaining the mixture in an ice bath to control the reaction rate. The resulting mixture was then stored in a refrigerator for 24 hours to ensure complete polymerization. The precipitate was subsequently filtered and washed multiple times with distilled water until a clear filtrate was obtained. Finally, the product was dried at 80 °C for 3 hours. Four different nanocomposite samples were thus prepared and stored for further characterization.

3. RESULTS AND DISCUSSIONS

3.1 X-Ray diffraction studies

The XRD patterns of pure polyaniline (PANI) and its nanocomposites doped with varying concentrations of silver oxide (Ag_2O) (10%, 15%, and 20% by weight) are presented in Figure 1. The diffraction pattern of pure PANI exhibits broad peaks centered around $2\theta \approx 18–25°$, which can be attributed to the (110), (200), (220), (211) and (111) planes of partially crystalline PANI domains. These broad peaks reflect the semi-crystalline nature of PANI, where ordered and disordered regions coexist along the polymer chains, a typical feature of conducting polymers (Rather et al., 2022).

Upon doping with Ag_2O at 10% concentration (PANI–Ag_2O–10S), the XRD pattern is dominated by sharp, intense diffraction peaks located at approximately 27.8°, 32.2°, 46.2°, 54.8°, 57.4°, 67.4°, 74.5°, 76.7°, and 85.6°. These peaks correspond to the (110), (111), (211), (220), (221), (310), (311), (222), and (321) planes of cubic Ag_2O phase. Remarkably, the characteristic broad peaks of PANI are not visible in this sample. This observation can be explained by the intrinsically low crystallinity of PANI and its broad diffraction features, which are easily masked by the sharper and higher intensity peaks of highly crystalline Ag_2O nanoparticles, even at relatively low concentrations. Additionally, the introduction of Ag_2O nanoparticles at 10% loading may disturb the packing of PANI chains, further reducing the formation of semi-crystalline domains detectable by XRD.

In contrast, the XRD patterns of the composites containing higher Ag_2O contents—15% (PANI–Ag_2O–15S) and 20% (PANI–Ag_2O–20S)—show both sets of reflections: the sharp peaks corresponding to crystalline Ag_2O and the broad peaks around 18–25° associated with PANI. This coexistence suggests that, at higher Ag_2O loading, the increased amount of inorganic phase enhances the overall crystallinity of the nanocomposite but also allows PANI chains to reorganize partially, maintaining their semi-crystalline domains. The presence of more Ag_2O may facilitate the formation

of more stable composite structures, in which the polymer matrix retains enough ordering to produce its characteristic diffraction pattern alongside the crystalline dopant.

The evolution of the XRD patterns with increasing Ag_2O concentration demonstrates a delicate interplay between dopant content, polymer chain organization, and composite crystallinity. At low doping levels, highly crystalline Ag_2O nanoparticles dominate the diffraction pattern and suppress the weaker PANI features, whereas at higher doping levels, the polymer matrix can partially reorganize around the larger number of inorganic particles, allowing both phases to be detected (Ali et al., 2023a; Rather et al., 2022).

The XRD analysis of pure PANI and its Ag_2O-doped composites shows a marked improvement in crystallinity and crystallite size upon doping. Pure PANI exhibited a low crystallinity of 21.2% and a small crystallite size of 49 nm, characteristic of its semi-crystalline polymeric nature. Incorporation of Ag_2O nanoparticles at 10%, 15%, and 20% concentrations increased the crystallinity to 68.3%, 77.4%, and 84.3%, respectively, with corresponding crystallite sizes rising to 213 nm, 267 nm, and 495 nm. This increase is attributed to the highly crystalline nature of Ag_2O, which dominates the XRD pattern and promotes the formation of larger crystalline domains within the composite. The results confirm that higher Ag_2O loading enhances the structural ordering of the material, potentially improving its functional properties (Gopal and Chellapandian, 2023; Gopal and Kannan, 2023; Lakshmi and Kannan, 2023).

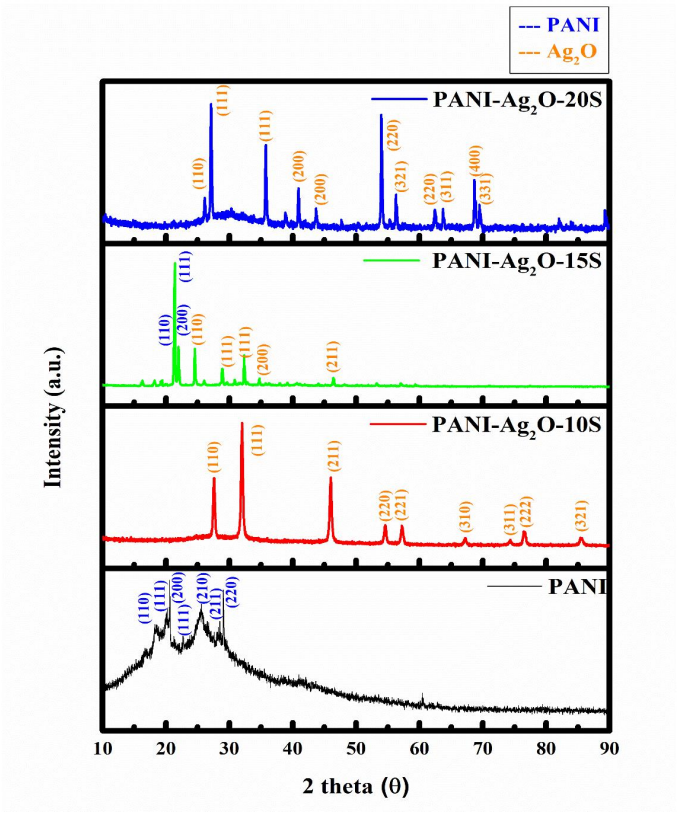

Figure 1. XRD pattern of pure Ag_2O and PANI–Ag_2O composites

3.2 UV–Visible Absorption, Band Gap Energy, and Urbach Energy Analysis

The optical properties of the synthesized Ag_2O and PANI-doped Ag_2O nanocomposites were investigated using UV–Visible spectroscopy in the wavelength range of 200–800 nm. The absorption spectra reveal significant differences in optical behavior between pure Ag_2O and the PANI-doped composite, attributed to the influence of the conjugated polymer on the semiconductor matrix.

4. 3.2.1 UV–VIS ABSORPTION ANALYSIS

The UV–Visible absorption spectra of Ag_2O displayed a strong and sharp absorption edge around 340–360 nm, indicative of electronic transitions from the valence band to the conduction band. Upon doping with polyaniline (PANI), a broadening and slight red-shift in the absorption edge were observed, extending absorption into the visible region. This is attributed to the presence of localized states introduced by the conductive polymer chains, which enhance the optical response and improve light-harvesting efficiency (Khalifeh, 2020).

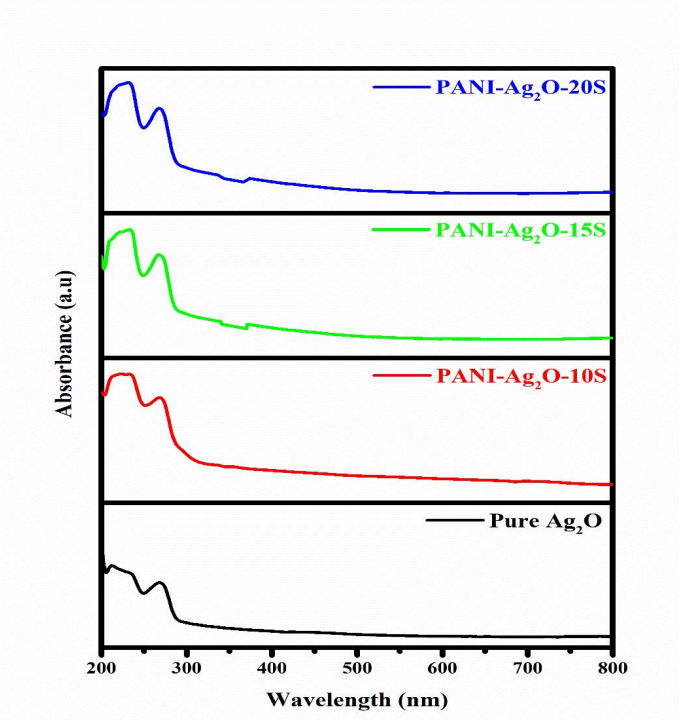

Figure 2 .UV-Visible absorption spectra of pure Ag_2O and PANI–Ag_2O composites

3.2.2 Band Gap Energy Determination

The band gap energy was calculated using Tauc plot analysis by plotting $(\alpha h\nu)^2$ against photon energy ($h\nu$). The extrapolation of the linear region to the x-axis yielded the optical band gap values. Both Ag_2O and PANI–Ag_2O nanocomposites exhibited a direct transition nature with band gap energy values calculated to be 3.63 eV for Ag_2O, 3.66 eV for PANI–Ag_2O-10S, 3.97 eV for PANI–Ag_2O-15S and 3.79 eV for PANI–Ag_2O-20S.

The increase in band gap upon PANI doping is primarily attributed to the protonation of polyaniline by hydrochloric acid (HCl), which converts the emeraldine base into its conductive emeraldine salt form. This protonation results in the formation of positively charged $–NH^+$ sites along the PANI chain, generating localized electrostatic potential barriers within the composite matrix. These potential barriers hinder the delocalization of charge carriers and necessitate higher photon energy for electronic transitions, leading to a blue shift in absorption edge and a wider optical band gap (Hadia et al., 2022; Zeng et al., 2020).

Additionally, the incorporation of PANI leads to surface passivation of Ag_2O nanoparticles, effectively suppressing mid-gap defect states and oxygen vacancies that would otherwise facilitate sub-bandgap transitions. This reduction in defect-assisted transitions enhances the purity of band-to-band excitations, thereby increasing the observed optical band gap (Behera, 2024).

At moderate PANI content (particularly 15 wt%), the presence of PANI also restricts particle growth, possibly introducing quantum confinement effects, which further elevate the energy levels of the conduction band. However, at higher PANI content (20 wt%), excess polymer coverage may introduce conductive networks or shield photon absorption, which can partially counteract the widening effect, resulting in a slight decrease in band gap from 3.97 to 3.79 eV.

These findings demonstrate that controlled doping of Ag_2O with HCl-protonated PANI can effectively tune its band gap properties, making such nanocomposites promising for UV-assisted photocatalytic applications and optoelectronic devices requiring wide band gap semiconductors.

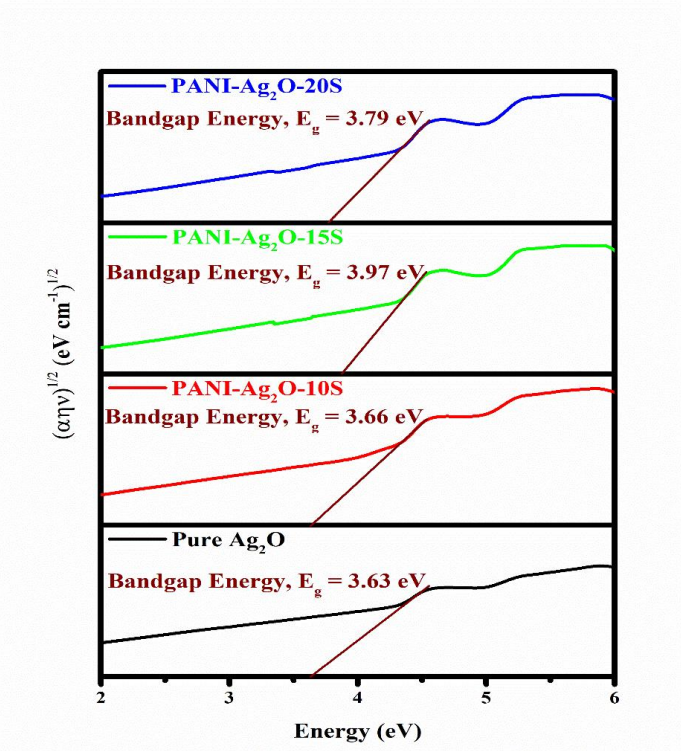

Figure 3. Bandgap energy plot of pure Ag_2O and PANI–Ag_2O composites

3.2.3 Urbach Energy Analysis

The Urbach energy (E_u) was derived from the exponential tail of the absorption spectra by plotting ln(α) against photon energy. The slope of the linear region was used to determine the degree of structural disorder and defect states in the materials. The Urbach energy was found to be 17.05 meV for Ag_2O, 9,09 meV for PANI–Ag_2O-10S, 6.38 meV for PANI–Ag_2O-15S and 6.02 meV for PANI–Ag_2O-20S.

The lower Urbach energy for PANI-doped Ag_2O indicates reduced defect states and improved structural order, possibly due to the passivation effect of the PANI chains, which bridge grain boundaries and suppress non-radiative recombination centers. This behavior suggests that the incorporation of PANI not only improves the light absorption characteristics but also enhances the electronic quality of the composite material (Qu et al., 2013).

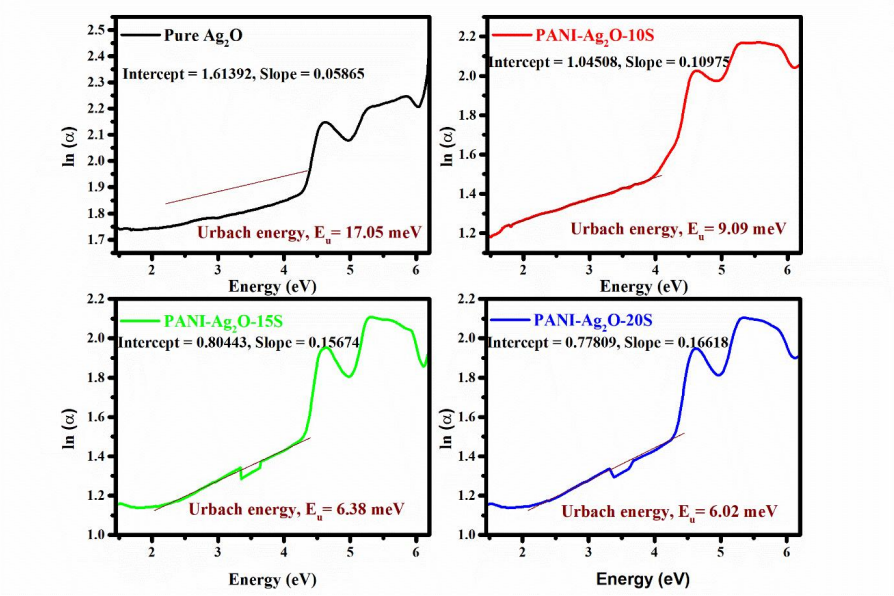

Figure 4. Urbach energy plot of of pure Ag_2O and PANI–Ag_2O composites

3.3 FTIR analysis

The FTIR spectra of pure Ag_2O and PANI-doped Ag_2O nanocomposites were recorded in the range of 4000–400 cm^{-1} to identify the functional groups present and to confirm the successful incorporation of polyaniline onto the silver oxide matrix. In the spectrum of pure Ag_2O, a prominent absorption band was observed around 550–600 cm^{-1}, which corresponds to the Ag–O stretching vibration, confirming the presence of silver oxide (Ali et al., 2023b, 2023a; Hadia et al., 2022).

Upon doping with PANI, additional bands appeared, which are characteristic of polyaniline's molecular structure. A sharp band around 1560–1590 cm^{-1} is attributed to the C=C stretching vibrations of the quinoid ring. A band near 1480–1500 cm^{-1} corresponds to the C=C stretching of the benzenoid ring. The peaks around 1300–1320 cm^{-1} are due to C–N stretching vibrations of the benzenoid unit. A peak at 1240–1260 cm^{-1} is associated with C–N^+ stretching vibration, indicative of polaron formation. The band at 1100–1140 cm^{-1} corresponds to the in-plane bending vibration of C–H, which also reflects the degree of doping in PANI (Hadia et al., 2022). A broad absorption band around 3400 cm^{-1} is attributed to O–H stretching from adsorbed moisture or possibly residual HCl used during synthesis (Ibrahim, 2017).

The successful doping of PANI into Ag_2O is confirmed by the presence of these characteristic PANI peaks along with the Ag–O vibrational band. A shift in peak positions and intensities was observed with increasing PANI content, which indicates a strong interaction between the polymer and metal oxide interface. This interaction can be attributed to hydrogen bonding, electrostatic interactions, and π–π stacking, which facilitate uniform dispersion of PANI onto the Ag_2O surface. Moreover, the presence of protons from the dopant (HCl) may contribute to enhanced conductivity and increased interaction at the interface, as evidenced by the sharpness and intensity of the C–N^+ peaks (Ibrahim, 2017). Overall, the FTIR analysis confirms the presence of Ag_2O, the successful incorporation of PANI and the formation of a composite with potential charge-transfer interactions.

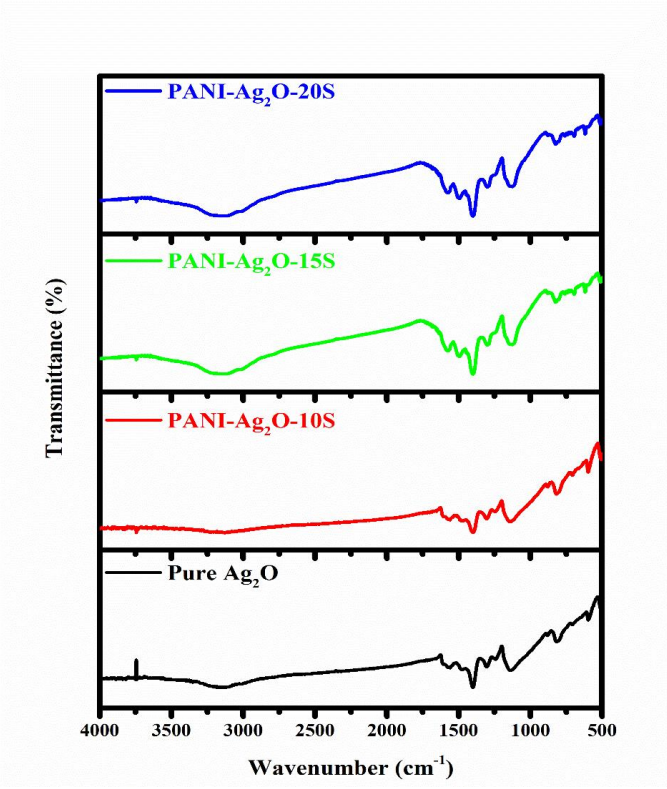

Figure 5.FT-IR spectra of pure Ag_2O and PANI–Ag_2O composites

3.4 Photocatalytic degradation of dyes

The photocatalytic degradation behavior of methylene blue and Congo red dyes was systematically investigated using Ag_2O and PANI-doped Ag_2O nanocomposites under visible-light irradiation. In the case of methylene blue, the degradation efficiency was initially low during the first 10 min, with values of 16.8%, 4.4%, 4.9% and 10.1% for Ag_2O, PANI–Ag_2O-10S, PANI–Ag_2O-15S and PANI–Ag_2O-20S, respectively. This stage was dominated by the adsorption of dye molecules on the catalyst surface. With continued irradiation, the degradation efficiency steadily increased. It was observed that Ag_2O showed superior performance in the early stages compared to its PANI-doped counterparts,

indicating that pure Ag_2O facilitated faster electron excitation and radical generation at the initial irradiation time. However, as the reaction progressed, the role of polyaniline became more pronounced. After 60 min of irradiation, the degradation efficiencies were 70.7%, 45.9%, 56.7% and 56.3% for Ag_2O, PANI–Ag_2O-10S, PANI–Ag_2O-15S and PANI–Ag_2O-20S, respectively. These results suggest that the incorporation of PANI did not significantly enhance the degradation of methylene blue and, in some cases, even suppressed it. The possible explanation is that excessive PANI coverage on the Ag_2O surface hindered the light absorption by the semiconductor and introduced additional recombination centers, thereby limiting the generation of active species required for methylene blue degradation (Suresh et al., 2023).

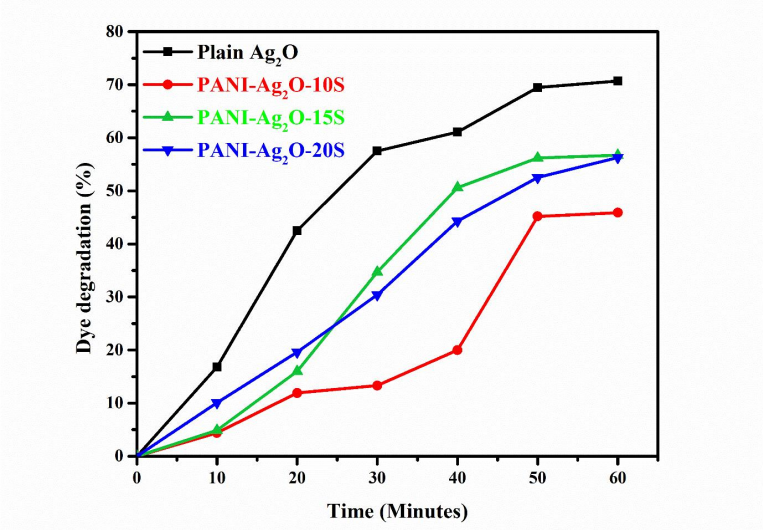

Figure 6. Photocatalytic degradation of Methylene by pure Ag_2O and PANI–Ag_2O composites

In contrast, Congo red degradation exhibited a different trend, with PANI incorporation playing a more beneficial role. At the initial 10 min, the efficiencies were 16.1%, 11.0%, 5.8% and 1.9% for Ag_2O, PANI–Ag_2O-10S, PANI–Ag_2O-15S and PANI–Ag_2O-20S, respectively, which reflects slow adsorption-dominated removal. Upon increasing time, the degradation efficiency gradually increases. But PANI–Ag_2O-10S degradation performance is very high compared to PANI–Ag_2O-15S, PANI–Ag_2O-20S and plain Ag_2O. The superior performance of the 10S sample can be attributed to an optimal level of polyaniline loading, which enhanced visible-light absorption, improved charge separation efficiency, and provided additional active sites through π–π interactions and electrostatic adsorption of dye molecules. On the other hand, the suppressed performance of the 15S and 20S samples at longer irradiation times suggests that excessive PANI may block the semiconductor's active surface, act as a recombination center, and reduce photon utilization, thereby limiting photocatalytic efficiency.

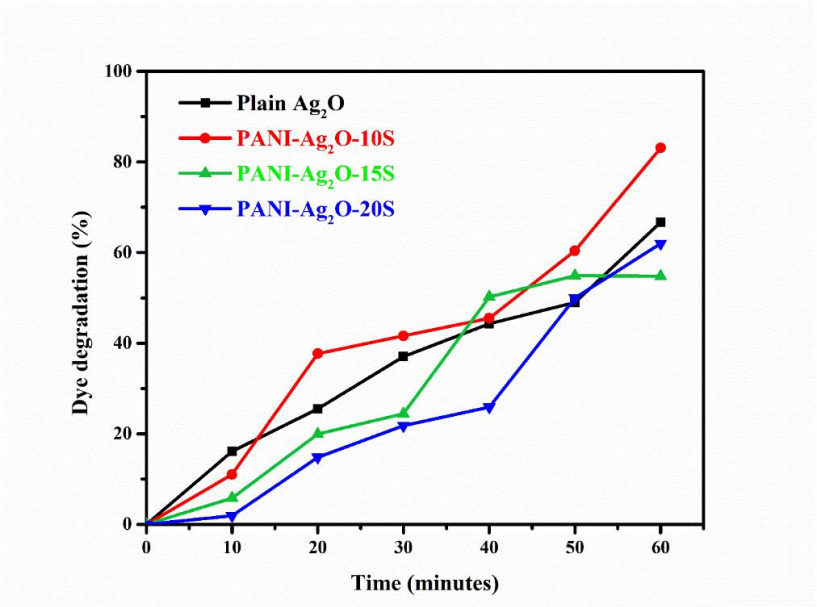

Figure 7. Photocatalytic degradation of Congo Red by pure Ag_2O and PANI–Ag_2O composites

These results suggested that the PANI–Ag_2O-10S has better degradation performance for both methylene blue and congo red dye. These observations are consistent with previous studies, which reported that conductive polymers such as polyaniline enhance photocatalytic efficiency by extending visible-light absorption and suppressing electron–hole recombination, but excessive coverage can passivate the surface and hinder active species formation (Boyer et al., 1998; Nagbasavanna et al., 2016; Porramezan and Eisazadeh, 2011).

3.5 Antibacterial activity by disc diffusion method

The antibacterial activity of Ag_2O and PANI–Ag_2O nanocomposites was evaluated against *Staphylococcus aureus* (Gram-positive), *Klebsiella pneumoniae* (Gram-negative), and *Pseudomonas aeruginosa* (Gram-negative) using the disc diffusion method. Chloramphenicol (10 µg/disc) served as the positive control and it is shown in Figure 4.7.

The results demonstrated that pure Ag_2O exhibited significant antibacterial activity, with inhibition zones approaching those of chloramphenicol in some cases. The strong activity of Ag_2O can be attributed to the release of Ag^+ ions, which interact with thiol groups of cellular enzymes, disrupt bacterial membranes, and promote the generation of reactive oxygen species (ROS), thereby inducing oxidative stress and bacterial cell death (Vi et al., 2020). Upon incorporation of PANI, the antibacterial performance showed a composition-dependent trend. PANI–Ag_2O–10S displayed moderate inhibition zones, suggesting that PANI facilitated enhanced interfacial contact between the nanocomposite and bacterial cells. However, at higher polymer loadings (PANI–Ag_2O–15S and 20S), the antibacterial activity decreased notably, likely due to polymer coverage of the Ag_2O surface, which reduced the release of Ag^+ ions and hindered ROS generation. This highlights the critical role of optimizing polymer dosage to maintain active surface sites while benefiting from the conductive polymer matrix (Wang et al., 2017). Chloramphenicol, the positive control, showed the largest inhibition zones for all tested strains, consistent with its known mechanism of action as a broad-spectrum antibiotic that inhibits protein synthesis by binding to the 50S ribosomal subunit (Li et al., 2014).

For *S. aureus*, the inhibition zone was highest at 0.2 M (15 mm) but remained substantially lower than the standard antibiotic (30 mm), reflecting moderate bactericidal action. *K. pneumoniae* showed a concentration-dependent trend, with the strongest inhibition observed at 0.4 M (15 mm), which nearly approached the standard value (18 mm), indicating a high susceptibility of this strain to Ag_2O. In contrast, *P. aeruginosa* displayed inconsistent results, with a maximum zone of 15 mm at 0.1 M but reduced inhibition at higher concentrations, possibly due to its intrinsic resistance mechanisms such as efflux pumps and biofilm formation.

Overall, the findings confirm that Ag_2O and PANI–Ag_2O composites possess significant antibacterial potential. However, excessive PANI doping reduces their efficiency, indicating that controlled loading is essential for balancing stability with bioactivity.

Table 1. Zone of inhibition (mm) of Ag_2O and PANI–Ag_2O nanocomposites against *Staphylococcus aureus*, *Klebsiella pneumoniae*, and *Pseudomonas aeruginosa* compared with chloramphenicol

Bacteria	0.1	0.2	0.3	0.4	Standard
Staphylococcus aureus	9	15	11	13	30
Klebsiella pneumoniae	9	13	12	15	18
Pseudomonas aeruginosa	15	9	12	12	20

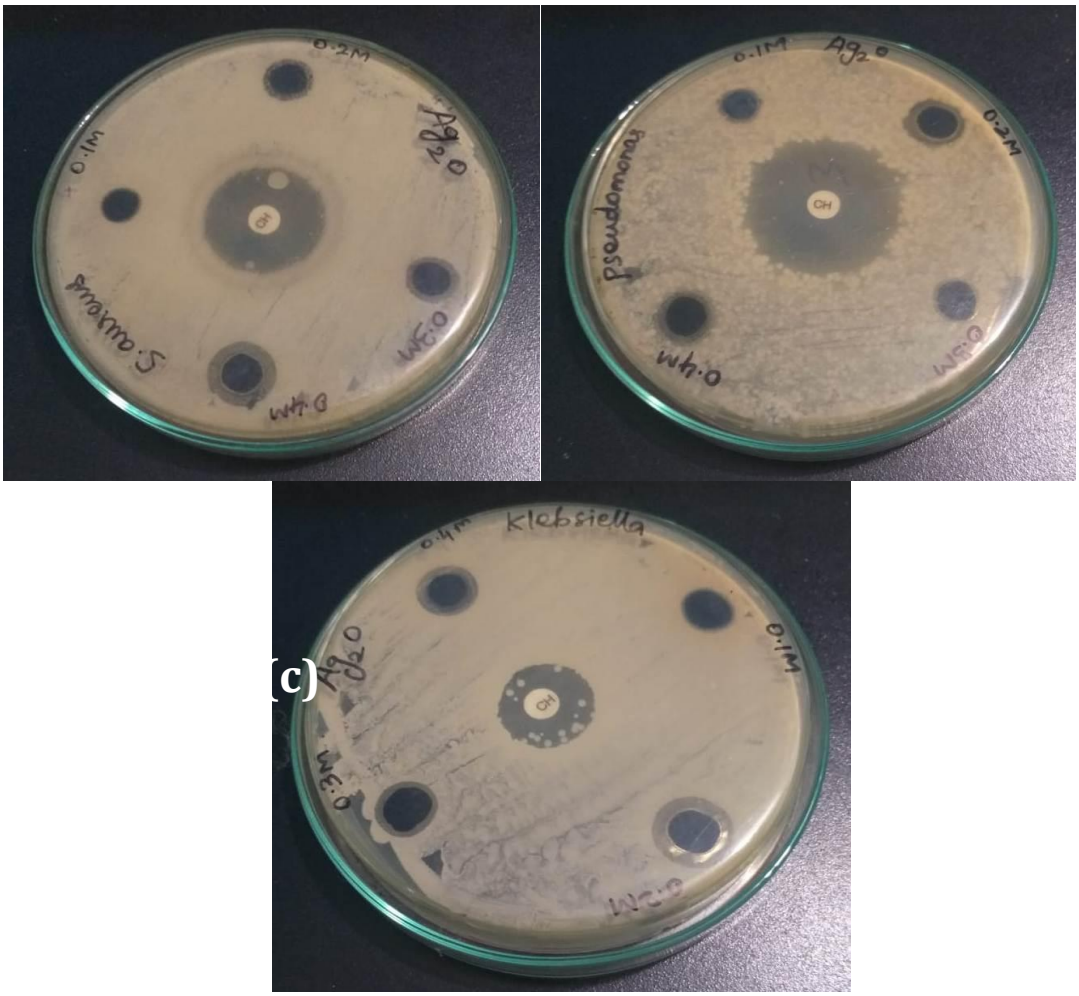

Figure 8 Antibacterial activity of Ag_2O and PANI–Ag_2O nanocomposites against pathogenic bacterial strains evaluated by the disc diffusion method. The inhibition zones are shown for (a) *Staphylococcus aureus*, (b) *Pseudomonas aeruginosa* and (c) *Klebsiella pneumoniae* with chloramphenicol (10 µg) used as the standard reference antibiotic for comparison.

3.6 Antifungal activity by disc diffusion method

The antifungal activity of Ag_2O nanoparticles was evaluated against *Candida albicans*, *Aspergillus niger*, and *Aspergillus flavus* using the disc diffusion method. The zones of inhibition were compared with the standard antibiotic chloramphenicol. The results clearly demonstrated concentration-dependent antifungal efficacy of Ag_2O.

For *C. albicans*, inhibition zones ranged between 9–16 mm, with the highest activity observed at 0.4 M Ag_2O (16 mm), although still lower than the standard antibiotic (20 mm). *A. niger* exhibited the strongest susceptibility at 0.2 M and 0.4 M, both recording 15–16 mm zones, suggesting a dose-dependent antifungal action. In the case of *A. flavus*, the inhibition zones (12–14 mm) were consistently lower than the standard (25 mm), but still indicated moderate antifungal potential. The standard chloramphenicol disc produced consistently larger zones of inhibition compared to Ag_2O, as expected due to its clinical potency. These findings are consistent with earlier reports that silver-based nanomaterials display potent antifungal activity by disrupting fungal cell walls, enhancing oxidative stress, and binding to intracellular components (Al-Soub et al., 2022; Fouda et al., 2022; Hashem et al., 2022; Hassan et al., 2019; Kazempour et al., 2013; Kim et al., 2009; Wang et al., 2017).

Overall, the results suggest that Ag_2O nanoparticles effectively suppress fungal growth, with activity increasing at higher concentrations. The mechanism can be attributed to silver ion release and reactive oxygen species (ROS) generation, which disrupt fungal cell membranes and metabolic processes. However, the zones of inhibition remained lower than the standard antibiotic, indicating that while Ag_2O has promising antifungal activity, further optimization (e.g., PANI-doping or surface functionalization) may be necessary to achieve clinical equivalence.

Table 2. Zone of inhibition (mm) of Ag_2O and PANI–Ag_2O nanocomposites against *Candida albicans*, *Aspergillus niger*, and *Aspergillus flavus* compared with chloramphenicol

Fungi	0.1	0.2	0.3	0.4	Standard
Candida albicans	12	12	9	16	20
Aspergillus niger	12	15	13	16	20
Aspergillus flavus	13	13	12	14	25

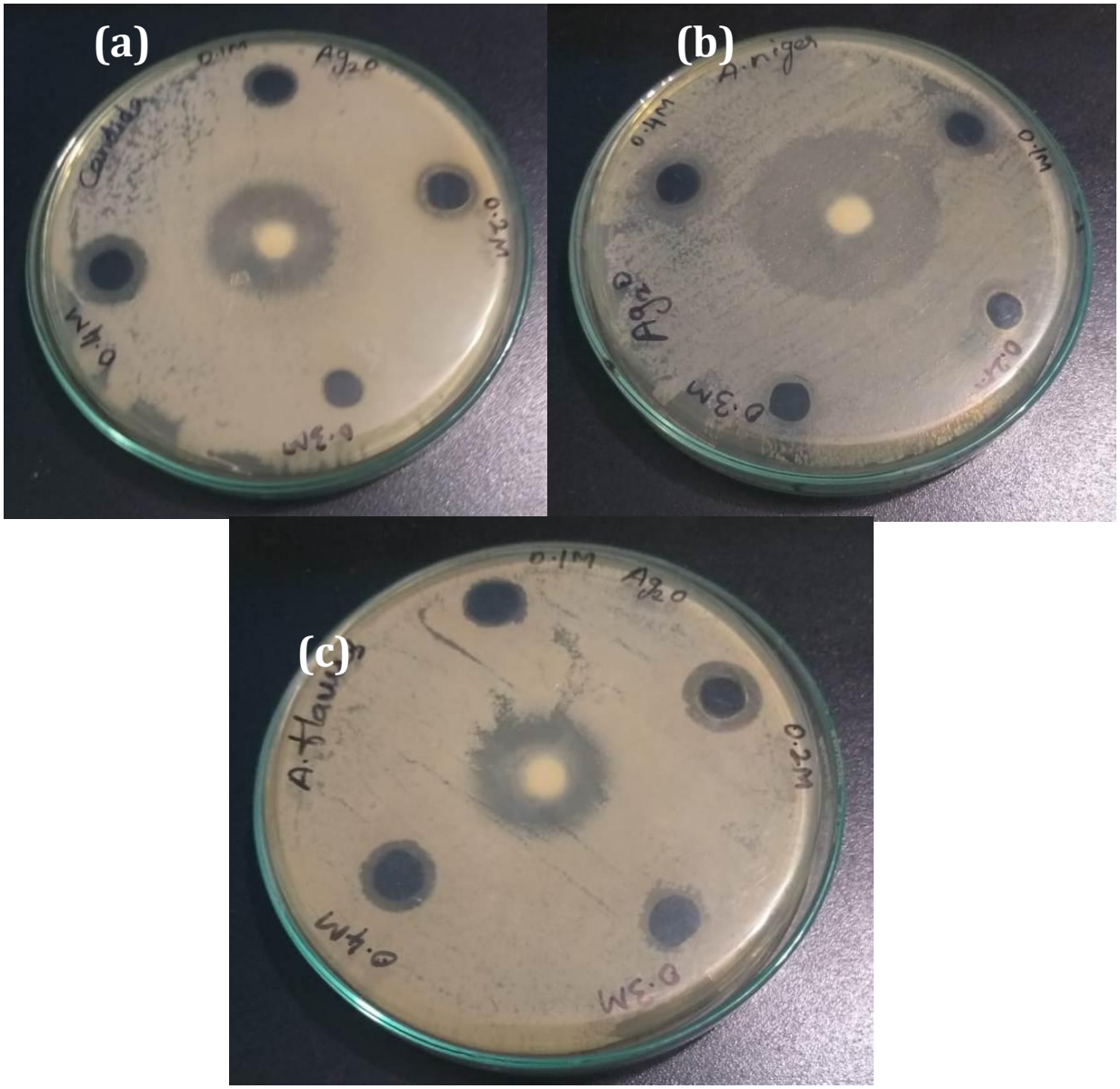

Figure 9. Antifungal activity of Ag_2O and PANI–Ag_2O nanocomposites against pathogenic bacterial strains evaluated by the disc diffusion method. The inhibition zones are shown for (a) *Candida albicans* (b) *Aspergillus niger* and (c) *Aspergillus flavus* with chloramphenicol (10 µg) used as the standard reference antibiotic for comparison.

5. CONCLUSION

The results of this study confirm the successful synthesis and multifunctional performance of PANI–Ag_2O nanocomposites. Characterization studies established that the incorporation of PANI modified the optical band gap

(3.63–3.97 eV), enhanced charge separation, and influenced structural features through strong interfacial interactions.

Photocatalytic studies demonstrated efficient degradation of methylene blue and congo red under visible light irradiation. Among the tested materials, PANI–Ag_2O-10S exhibited the highest degradation efficiency, attributed to optimized polymer loading that promoted electron–hole separation while preventing excessive surface shielding. However, higher doping levels (PANI–Ag_2O-15S and PANI–Ag_2O-20S) led to reduced photocatalytic activity due to polymer-induced site blocking. These findings highlight the importance of dosage optimization in achieving maximum catalytic efficiency.

The antimicrobial assays further validated the bioactive potential of the synthesized materials. Ag_2O displayed significant antibacterial and antifungal activity, while PANI–Ag_2O composites exhibited enhanced inhibition against Gram-positive and Gram-negative bacteria, as well as pathogenic fungi. The activity was, however, dependent on the PANI loading, with excessive polymer content reducing silver ion availability and lowering inhibition efficiency. Comparison with the standard antibiotic chloramphenicol confirmed that, while conventional drugs remain superior, the nanocomposites provide promising alternative antimicrobial platforms with multi-mechanistic modes of action.

In summary, this chapter demonstrated that PANI–Ag_2O nanocomposites exhibit dual functionality as efficient photocatalysts for dye degradation and as potent antimicrobial agents. Their combined environmental and biomedical potential makes them highly relevant for addressing pressing challenges in wastewater treatment and microbial resistance. Future work should explore detailed mechanistic pathways, long-term stability, and cytotoxicity studies to further advance their application in real-world systems.

REFERENCES

[1] Abirami S, E K. A review on metal oxide-doped polyaniline nanocomposites. J Mater Sci 2024;59:1–31. https://doi.org/10.1007/s10853-024-10020-z.

[2] Ali ZM, Murshed MN, El Sayed ME, Samir A, Alsharabi RM, Farea MO. A new fabrication strategy of Ag2O doped PANI as a highly stable and room temperature operable carbon monoxide gas sensor. Opt Mater (Amst) 2023a;144:114324. https://doi.org/10.1016/J.OPTMAT.2023.114324.

[3] Ali ZM, Murshed MN, El Sayed ME, Samir A, Alsharabi RM, Farea MO. A new fabrication strategy of Ag2O doped PANI as a highly stable and room temperature operable carbon monoxide gas sensor. Opt Mater (Amst) 2023b;144:114324. https://doi.org/10.1016/J.OPTMAT.2023.114324.

[4] Al-Soub A, Khleifat K, Al-Tarawneh A, Al-Limoun M, Alfarrayeh I, Sarayreh A Al, et al. Silver nanoparticles biosynthesis using an airborne fungal isolate, Aspergillus flavus: optimization, characterization and antibacterial activity. Iran J Microbiol 2022;14:518–28. https://doi.org/10.18502/ijm.v14i4.10238.

[5] Behera S. A Review on Polyaniline-Supported Catalyst for Organic Transformations. ACS Omega 2024;9:50097–117. https://doi.org/10.1021/acsomega.4c04352.

[6] Boyer M-I, Quillard S, Rebourt E, Louarn G, Buisson JP, Monkman A, et al. Vibrational Analysis of Polyaniline: A Model Compound Approach. J Phys Chem B 1998;102:7382–92. https://doi.org/10.1021/jp972652o.

[7] Fouda A, Awad MA, AL-Faifi ZE, Gad ME, Al-Khalaf AA, Yahya R, et al. Aspergillus flavus-Mediated Green Synthesis of Silver Nanoparticles and Evaluation of Their Antibacterial, Anti-Candida, Acaricides, and Photocatalytic Activities. Catalysts 2022;12. https://doi.org/10.3390/catal12050462.

[8] Gopal VL, Chellapandian K. Synthesis of hybrid framework of tenorite and octahedrally coordinated aluminosilicate for the robust adsorption of cationic and anionic dyes. Environ Res 2023;220:115111. https://doi.org/10.1016/j.envres.2022.115111.

[9] Gopal VL, Kannan C. Room temperature fabrication of cobalt mullite for the snappy adsorption of cationic and anionic dyes. Environmental Science and Pollution Research 2023;30:67788–803. https://doi.org/10.1007/s11356-023-27067-1.

[10] Hadia NMA, Hajjiah A, Elsayed AM, Mohamed SH, Alruqi M, Shaban M, et al. Bunch of Grape-Like Shape PANI/Ag2O/Ag Nanocomposite Photocatalyst for Hydrogen Generation from Wastewater. Adsorption Science and Technology 2022;2022. https://doi.org/10.1155/2022/4282485.

[11] Hashem AH, Saied E, Amin BH, Alotibi FO, Al-Askar AA, Arishi AA, et al. Antifungal Activity of Biosynthesized Silver Nanoparticles (AgNPs) against Aspergilli Causing Aspergillosis: Ultrastructure Study. J Funct Biomater 2022;13. https://doi.org/10.3390/jfb13040242.

[12] Hassan SA, Hanif E, Khan UH, Tanoli AK. Antifungal activity of silver nanoparticles from Aspergillus niger. Pak J Pharm Sci 2019;32:1163–6.

[13] Ibrahim KA. Synthesis and characterization of polyaniline and poly(aniline-co-o-nitroaniline) using vibrational spectroscopy. Arabian Journal of Chemistry 2017;10:S2668–74.

https://doi.org/10.1016/J.ARABJC.2013.10.010.

[14] Kazempour ZB, Yazdi MH, Rafii F, Shahverdi AR. Sub-inhibitory concentration of biogenic selenium nanoparticles lacks post antifungal effect for Aspergillus niger and Candida albicans and stimulates the growth of Aspergillus niger. Iran J Microbiol 2013;5:81–5.

[15] Khalifeh S. OPTIMIZATION OF ELECTRICAL, ELECTRONIC AND OPTICAL PROPERTIES OF ORGANIC ELECTRONIC STRUCTURES. Polymers in Organic Electronics 2020:185–202. https://doi.org/10.1016/B978-1-927885-67-3.50009-2.

[16] Kim K-J, Sung WS, Suh BK, Moon S-K, Choi J-S, Kim JG, et al. Antifungal activity and mode of action of silver nano-particles on Candida albicans. BioMetals 2009;22:235–42. https://doi.org/10.1007/s10534-008-9159-2.

[17] Kumar H, Boora A, Yadav A, Rajni, Rahul. Polyaniline-metal oxide-nano-composite as a nano-electronics, opto-electronics, heat resistance and anticorrosive material. Results Chem 2020;2:100046. https://doi.org/10.1016/J.RECHEM.2020.100046.

[18] Kumar R, Umar A, Kumar G, Nalwa HS. Antimicrobial Properties of ZnO Nanomaterials: A Review. Ceram Int 2017;43:3940–61. https://doi.org/10.1016/j.ceramint.2016.12.062.

[19] Lakshmi GV, Kannan C. A novel integrated multiphase crystal system of Kavlite for the effective and instantaneous removal of cationic and anionic dyes. Surfaces and Interfaces 2023;40:103113. https://doi.org/10.1016/J.SURFIN.2023.103113.

[20] Li X, Robinson SM, Gupta A, Saha K, Jiang Z, Moyano DF, et al. Functional gold nanoparticles as potent antimicrobial agents against multi-drug-resistant bacteria. ACS Nano 2014;8:10682–6. https://doi.org/10.1021/nn5042625.

[21] Nagbasavanna D, Guragol S, Limbitot M, Kalyane S, Sharanappa N, Lagali K. Synthesis and Characterization of Ag 2 O Doped Polyaniline. International Journal on Emerging Technologies (Special Issue on ICRIET-2016) 2016;7:207–11.

[22] Porramezan M, Eisazadeh H. Fabrication and characterization of polyaniline nanocomposite modified with Ag2O nanoparticles. Compos B Eng 2011;42:1980–6. https://doi.org/10.1016/J.COMPOSITESB.2011.05.029.

[23] Qu X, Lü S, Jia D, Zhou S, Meng Q. First-principles study of the electronic structure of Al and Sn co-doping ZnO system. Mater Sci Semicond Process 2013;16:1057–62. https://doi.org/10.1016/J.MSSP.2013.04.002.

[24] Rather MH, Mir FA, Ullah F, Bhat MA, Najar FA, Shakeel G, et al. “Polyaniline nanoparticles: A study on its structural, optical, electrochemical properties along with some possible device applications.” Synth Met 2022;290:117152. https://doi.org/10.1016/J.SYNTHMET.2022.117152.

[25] Shivhare S, Vyas S. Polyaniline (PANI) Metal Oxide Nano Composites as a Conducting Material. International Journal of Research and Scientific Innovation 2017;Volume IV:86–9.

[26] Suresh S, Alshahateet S, Lett A, Fatimah I, Sivasankaran R, Sibhatu A, et al. Highly efficient photocatalytic degradation of methylene blue dye over Ag2O nanoparticles under solar light irradiation. Inorg Chem Commun 2023;148:110288. https://doi.org/10.1016/j.inoche.2022.110288.

[27] Thenmozhi M, Kannabiran K, Kumar R, Gopiesh Khanna V. Antifungal activity of Streptomyces sp. VITSTK7 and its synthesized Ag2O/Ag nanoparticles against medically important Aspergillus pathogens. J Mycol Med 2013;23:97–103. https://doi.org/10.1016/J.MYCMED.2013.04.005.

[28] Vi TTT, Kumar SR, Pang J-HS, Liu Y-K, Chen DW, Lue SJ. Synergistic Antibacterial Activity of Silver-Loaded Graphene Oxide towards Staphylococcus Aureus and Escherichia Coli. Nanomaterials 2020;10. https://doi.org/10.3390/nano10020366.

[29] Wang B, Han X, Bai Y, Lin Z, Qiu M, Nie X, et al. Effects of nitrogen metabolism on growth and aflatoxin biosynthesis in Aspergillus flavus. J Hazard Mater 2017;324:691–700. https://doi.org/10.1016/J.JHAZMAT.2016.11.043.

[30] Zeng Q, Guo S, Sun Y, Li Z, Feng W. Protonation-induced enhanced optical-light photochromic properties of an inorganic-organic phosphomolybdic acid/polyaniline hybrid thin film. Nanomaterials 2020;10:1–18. https://doi.org/10.3390/nano10091839.